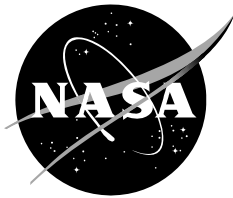# Mathematical Characterization of Battery Models

Kenneth W. Eure
Langley Research Center Hampton, Virginia

Edward F. Hogge
National Institute of Aerospace, Hampton, Virginia

NASA STI Program Report Series

Since its founding, NASA has been dedicated to the advancement of aeronautics and space science. The NASA scientific and technical information (STI) program plays a key part in helping NASA maintain this important role.

The NASA STI program operates under the auspices of the Agency Chief Information Officer. It collects, organizes, provides for archiving, and disseminates NASA's STI. The NASA STI program provides access to the NTRS Registered and its public interface, the NASA Technical Reports Server, thus providing one of the largest collections of aeronautical and space science STI in the world. Results are published in both non-NASA channels and by NASA in the NASA STI Report Series, which includes the following report types:

- TECHNICAL PUBLICATION. Reports of completed research or a major significant phase of research that present the results of NASA Programs and include extensive data or theoretical analysis. Includes compilations of significant scientific and technical data and information deemed to be of continuing reference value. NASA counterpart of peer-reviewed formal professional papers but has less stringent limitations on manuscript length and extent of graphic presentations.

- TECHNICAL MEMORANDUM. Scientific and technical findings that are preliminary or of specialized interest, e.g., quick release reports, working papers, and bibliographies that contain minimal annotation. Does not contain extensive analysis.

- CONTRACTOR REPORT. Scientific and technical findings by NASA-sponsored contractors and grantees.

- CONFERENCE PUBLICATION. Collected papers from scientific and technical conferences, symposia, seminars, or other meetings sponsored or co-sponsored by NASA.

- SPECIAL PUBLICATION. Scientific, technical, or historical information from NASA programs, projects, and missions, often concerned with subjects having substantial public interest.

- TECHNICAL TRANSLATION. English-language translations of foreign scientific and technical material pertinent to NASA's mission.

Specialized services also include organizing and publishing research results, distributing specialized research announcements and feeds, providing information desk and personal search support, and enabling data exchange services.

For more information about the NASA STI program, see the following:

- Access the NASA STI program home page at http://www.sti.nasa.gov

- Help desk contact information:

https://www.sti.nasa.gov/sti-contact-form/
and select the "General" help request type.

NASA/TM-20205008059
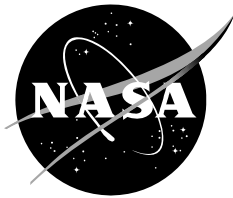
Mathematical Characterization of Battery Models

Kenneth W. Eure
Langley Research Center, Hampton Virginia

Edward F. Hogge
National Institute of Aerospace, Hampton, Virginia

National Aeronautics and
Space Administration

Langley Research Center
Hampton, VA 23681

January 2021

Acknowledgments

Available from:

NASA STI Program / Mail Stop 148
NASA Langley Research Center
Hampton, VA 23681-2199
Fax: 757-864-6500

Contents

Abstract

The purpose of this document is to demonstrate the use of the Extended Kalman Filter as a tool for battery state estimation and the estimation of battery state of charge. The mathematical details based on the equivalent circuit model are presented followed by an electrochemical engineering model. A simplified first-order model is used to demonstrate the procedure followed by second and third-order models. Next a simplified electrochemistry model is presented along with observer development. State observability is calculated for the simpler equivalent circuit models and the simplified electrochemistry model. An outline of the battery model parameter identification method is presented, and model performance based on experimental and flight data is demonstrated.

Introduction

Kalman filtering is an established technology used since the Apollo program for the estimation of states within a dynamic system. For linear systems, this method of state estimation is optimal. The Kalman filter consists of a set of recursive equations that are evaluated repeatedly and updated using input/output measurements as the system operates. This recursion allows for real-time tracking of the state as new data become available. For linear observable systems with known process and measurement noise variances, the Kalman filter has been widely employed as the optimal state estimator. However, many systems are nonlinear. In our case, the battery discharge voltage profile is a nonlinear function of the input current demand. In order to approximate an application of the Kalman filter to nonlinear systems, the extended Kalman filter (EKF) has been developed. The EKF is derived from the nonlinear system equations by representing the nonlinear system using the first term of the nonlinear equation's Taylor series expansion. This makes development of the Kalman filter possible for nonlinear systems but sacrifices system representation by employing an approximate (linear) model. For battery modeling, the EKF has been used for state observation of nonlinear battery models [1]. However, the development of the EKF involves taking derivatives that may be complex and prone to mathematical computational errors.

State observers are used to update battery state estimates based on observations of current and voltage at the battery output terminals. An equivalent circuit battery model in [2] [3] is used to represent battery terminal voltage dynamics as a function of battery current. The model is based on Thevenin's theorem to model the current and voltage profile of the battery as a black box input-output device. A first-approximation assumption is made such that the battery state can match a linear electrical network with voltage and current sources and only resistances. Thevenin states that the black box can be replaced at the input output terminals by an equivalent voltage source in series connection with an equivalent resistance. To better match standard battery phenomena, such as internal resistance voltage drops and hysteresis effects, additional pairs of series connected RC parallel circuits are added to the model. The R_s, C_s pair are added for the internal resistance drop and the R_{sp}, C_{sp} pair are added for the concentration polarization effect. These additional terms help to model battery nonlinearities. The correspondence of these RC circuits to actual battery chemical phenomena is only notional. In the equivalent circuit model, some of the components were made to vary according to the bulk charge stored in C_b. The State of Charge (SOC) is an estimate of the battery bulk charge. The battery input-output voltage dynamics will change as a function of this bulk charge estimate. Battery SOC is defined here as:

$$SOC = 1 - \frac{q_{max} - q_b}{C_{max}}$$

where q_b represents the charge stored in capacitor C_b, q_{max} is the maximum charge that the battery can hold, and C_{max} is the maximum charge that can be drawn from the battery in practice.

Model-based battery SOC estimation has been developed here using an equivalent circuit representation [2]. Various methods of analyses for performance and conditions under which the model state is observable have been proposed and demonstrated using simulated and experimental battery data [4]. The Extended Kalman Filter, EKF, has been analyzed and demonstrated in tutorials including detail development and discussion [1]. The purpose of this paper is to examine the equivalent circuit model using the Extended Kalman Filter, EKF, as the state observer and apply the methods to the electrochemistry model, EchM. Some discussion will be presented regarding the condition where state observability may be expected. This paper first presents a mathematical development of the first, second, and third-order EKF models followed by a section on simulations. Performance of the model with simulated data is given. Application of the model with flight data is then presented to further illustrate the concepts developed.

3. Battery Models and Observers

This section contains the battery models and details the development of the EKF observers for each model. The equivalent circuit model, ECM, is presented first followed by a simplified electrochemical model. For the lower order models, the EKF is developed and comments are made concerning observability. For each of the models the meaning of the model variables and the physics represented, if any, will not be detailed here. The reader may find these in the cited publications.

3.1 First-Order Equivalent Circuit Model

Consider the first-order continuous time equivalent circuit model shown in Figure 1 [2]. The first-order continuous time approximation to this circuit is shown in equation set (1) where only circuit component C_b is considered. Here $\dot{q}_b(t)$ is the rate of change of the charge on C_b, $i(t)$ is
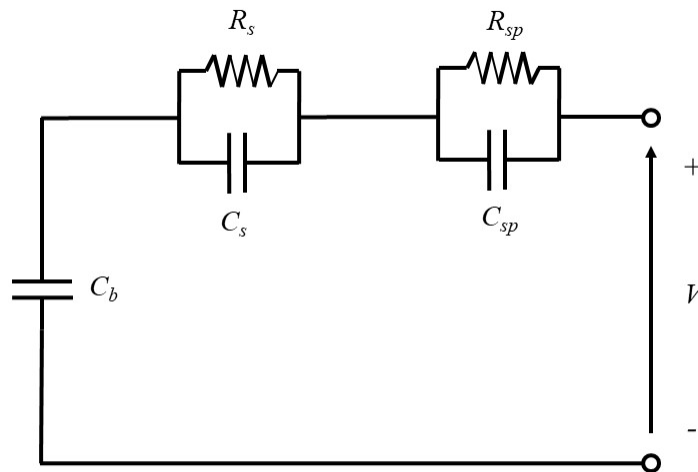

Figure 1. Equivalent Circuit Model.

the current delivered by the battery, q_{max} is the maximum possible charge, C_{max} is the maximum possible battery capacity, and the coefficients C_0, C_1, C_2, and C_3 model the nonlinear relationship between SOC and battery output voltage $V(t)$. The continuous time state equation is denoted as f_c and output equation as h_c.

2

$$\dot{q}_b(t) = -i(t) = f_c$$

$$SOC(t) = 1 - \frac{q_{max} - q_b(t)}{C_{max}}$$

$$C_b = C_0 SOC(t)^3 + C_1 SOC(t)^2 + C_2 SOC(t) + C_3$$

$$V(t) = \frac{q_b(t)}{C_b} = h_c \tag{1}$$

In discrete-time the model becomes as shown in (2) where k is the time step and T_s the sample period.

$$q_b(k) = q_b(k-1) - i(k)T_s = f$$

$$SOC(k) = 1 - \frac{q_{max} - q_b(k)}{C_{max}}$$

$$C_b = C_0 SOC(k)^3 + C_1 SOC(k)^2 + C_2 SOC(k) + C_3$$

$$V(k) = \frac{q_b(k)}{C_b} = h \tag{2}$$

In model (2) we have a first order state equation $q_b(k)$ and a single output equation $V(k)$. Although the state equation is linear in terms of charge $q_b(k)$, the voltage $V(k)$ output equation h is clearly nonlinear. The EKF requires that we take the Jacobian of the state and output equations [1]. In the equations below, $x = q_b$ is the state and the discrete-time state equation f is $q_b(k-1) - i(k)T_s$. The discrete-time output equation is h. Here we have suppressed the time step index for ease of presentation.

$$F = \frac{\partial f}{\partial x} = 1$$

$$H = \frac{\partial h}{\partial x} = \frac{\partial}{\partial x}\left\{\frac{x}{C_b}\right\} = \frac{\partial x/\partial x\, C_b - x\, \partial C_b/\partial x}{C_b^2} \tag{3}$$

In determining (3) the quotient rule was used. We next use the chain rule to complete the Jacobian.

$$\partial C_b/\partial x = 3C_0 SOC^2\, \partial SOC/\partial x + 2C_1 SOC\, \partial SOC/\partial x + C_2\, \partial SOC/\partial x$$

$$\partial SOC/\partial x = \partial/\partial x\{1 - q_{max}/C_{max} + x/C_{max}\} = 1/C_{max} \tag{4}$$

Combining (3) and (4) we arrive at the expression for H as shown in (5).

$$\partial C_b/\partial x = 1/C_{max}\{3C_0 SOC^2 + 2C_1 SOC + C_2\}$$

$$H = \frac{C_b - x\, \partial C_b/\partial x}{C_b^2} \tag{5}$$

The EKF may be implemented using the equations for F and H.

Prediction (Time Update) $x(k+1) = f(x(k), i(k))$

$$P = FPF^T + Q$$

Update (Measurement) $V_e(k) = h(x(k))$

3

$$x(k + 1) = x(k + 1) + PH^T(HPH^T + R)^{-1}(V(k) - V_e(k))$$

$$P = P - PH^T(HPH^T + R)^{-1}HP \tag{6}$$

Equation set (6) may be used to estimate the state x for the given first order battery model. Here we have voltage measurements $V(k)$, estimated voltages $V_e(k)$, system process noise covariance Q, measurement noise R, and state covariance P. It is of interest to determine the conditions under which the state is observable. To do so we perform an observability analysis [4].

The observability matrix for a nonlinear system may be found by taking the Jacobian of the observable coordinates. This is performed using the continuous time model of equation set (1). For this simple case the observability coordinate is the output equation and the Jacobian is the derivative with respect to the state. For the first order continuous time system of equation (1) we have equation (7).

$$Obv = \left[\frac{\partial}{\partial q_b}\left\{\frac{q_b}{C_b}\right\}\right] = \frac{1}{C_b} - \frac{q_b}{C_b^2}(3C_0 SOC^2 + 2C_1 SOC + C_2)\frac{1}{C_{Max}} \tag{7}$$

Since (7) is a scalar, the points where the state becomes unobservable occur are when Obv approaches zero. A small Obv indicates the state is weakly observable.

3.2   Second-Order Model

The first-order equivalent circuit model is expanded by the addition of several more components of [2] as shown in (8) for continuous time. Here the components R_{sp} and C_{sp} capture the battery electrode surface overpotential and the equation for R_{sp} captures this nonlinear relationship in an empirical form [2]. The R_{sp} and C_{sp} pair time constant models the slow relaxation voltage recovery once a load is removed.

$$\dot{q}_b(t) = -i(k) = f_{1c}$$

$$\dot{q}_{sp}(t) = i(t) - q_{sp}(t)/(C_{sp}R_{sp}(t)) = f_{2c}$$

$$SOC(t) = 1 - \frac{q_{max} - q_b(t)}{C_{max}}$$

$$R_{sp}(t) = R_{sp0} + R_{sp1}\exp\left(R_{sp2}(1 - SOC(t))\right)$$

$$C_b(t) = C_0 SOC(t)^3 + C_1 SOC(t)^2 + C_2 SOC(t) + C_3$$

$$V(t) = \frac{q_b(t)}{C_b} - \frac{q_{sp}(t)}{C_{sp}} \tag{8}$$

The discrete-time model is shown in (9) below.

$$q_b(k) = q_b(k - 1) - i(k)T_s = f_1$$

$$q_{sp}(k) = \exp\left(\frac{-T_s}{C_{sp}R_{sp}(k)}\right)q_{sp}(k - 1) + C_{sp}R_{sp}(t)\left(1 - \exp\left(\frac{-T_s}{C_{sp}R_{sp}(k)}\right)\right) = f_2$$

$$SOC(k) = 1 - \frac{q_{max} - q_b(k)}{C_{max}}$$

4

$$R_{sp}(k) = R_{sp0} + R_{sp1}\exp\left(R_{sp2}(1 - SOC(k))\right)$$

$$C_b(k) = C_0 SOC(k)^3 + C_1 SOC(k)^2 + C_2 SOC(k) + C_3$$

$$V(k) = \frac{q_b(k)}{C_b} - \frac{q_{sp}(k)}{C_{sp}} \tag{9}$$

Here we have the states $x_1 = q_b$ and $x_2 = q_{sp}$ forming the state vector $f = [x_1 \quad x_2]^T$. As with the first-order system, we can now compute the Jacobians needed for the EKF as shown in (10) and (11). This is done using the approximate discrete-time model where the continuous-time derivative is simply replaced by Euler integration. This can be done because the sampling rate is much faster than the battery dynamics. We have the approximation

$$\dot{q}_b(t) \approx \left(q_b(k) - q_b(k-1)\right)/T_s \text{ and } \dot{q}_{sp}(t) \approx \left(q_{sp}(k) - q_{sp}(k-1)\right)/T_s.$$

$$F = \frac{\partial f}{\partial x} = \begin{bmatrix} \frac{\partial f_1}{\partial x_1} & \frac{\partial f_1}{\partial x_2} \\ \frac{\partial f_2}{\partial x_1} & \frac{\partial f_2}{\partial x_2} \end{bmatrix} = \begin{bmatrix} 1 & 0 \\ \frac{\partial f_2}{\partial x_1} & 1 - \frac{T_s}{C_{sp}R_{sp}} \end{bmatrix}$$

$$\frac{\partial f_2}{\partial x_1} = \frac{x_2 T_s}{C_{sp}R_{sp}^2}\left(\frac{\partial R_{sp}}{\partial x_1}\right)$$

$$\frac{\partial R_{sp}}{\partial x_1} = -R_{sp1}R_{sp2}\exp\{R_{sp2}(1 - SOC)\}\frac{\partial SOC}{\partial x_1}$$

$$\frac{\partial SOC}{\partial x_1} = \frac{1}{C_{max}}$$

$$\frac{\partial f_2}{\partial x_1} = \frac{x_2 T_s}{C_{sp}R_{sp}^2}\left[-R_{sp1}R_{sp2}\exp\{R_{sp2}(1 - SOC)\}\frac{1}{C_{max}}\right] \tag{10}$$

Likewise, from the output equation we compute *H* as shown in (11).

$$H = \frac{\partial h}{\partial x} = \frac{\partial V}{\partial x} = \frac{\partial}{\partial x}\left(\frac{x_1}{C_b} - \frac{x_2}{C_{sp}}\right) = \begin{bmatrix} \frac{\partial}{\partial x_1}\left(\frac{x_1}{C_b}\right) & -\frac{1}{C_{sp}} \end{bmatrix}$$

$$\frac{\partial}{\partial x_1}\left(\frac{x_1}{C_b}\right) = \frac{C_b - x_1\frac{\partial C_b}{\partial x_1}}{C_b^2}$$

$$\frac{\partial C_b}{\partial x_1} = \{3C_0 SOC^2 + 2C_1 SOC + C_2\}\frac{1}{C_{max}} \tag{11}$$

Equations (9), (10) and (11) may be used to form the EKF as shown in algorithm (6).

The observability matrix for the second order system may be computed as for the first-order system. Consider the continuous-time system of equation (8) where the output is $y = V$ and the Lie derivative [4] of $h(\zeta)$ along $f(\zeta)$ is $L_f h(\zeta) = (\partial h(\zeta)/\partial \zeta)f(\zeta)$. In our case ζ is the state *x*, *h* is the output equation and *f* is the state equation. We first form the observable coordinates as shown in equation (12).

$$y = \frac{x_1}{C_b} - \frac{x_2}{C_{sp}}$$

$$L_f y = \frac{\partial h}{\partial x} f = \frac{\partial}{\partial x} \left\{ \frac{x_1}{C_b} - \frac{x_2}{C_{sp}} \right\} \begin{bmatrix} f_1 \\ f_2 \end{bmatrix} = \left[\frac{\partial}{\partial x_1} \left(\frac{x_1}{C_b} \right) \quad -\frac{1}{C_{sp}} \right] \left[\frac{-x_2}{C_{sp} R_{sp}} + i \right]$$

$$L_f y = \left\{ \frac{x_1}{C_b^2 C_{Max}} (3C_0 SOC^2 + 2C_1 SOC + C_2) - \frac{1}{C_b} \right\} i + \frac{x_2}{C_{sp}^2 R_{sp}} - \frac{i}{C_{sp}} \qquad (12)$$

We next take the Jacobian of the observable coordinates y and $L_f y$ to form the observability matrix as given in equation (13).

$$Obv = \nabla \begin{pmatrix} y \\ L_f y \end{pmatrix} = \begin{bmatrix} \frac{\partial y}{\partial x_1} & \frac{\partial y}{\partial x_2} \\ \frac{\partial L_f y}{\partial x_1} & \frac{\partial L_f y}{\partial x_2} \end{bmatrix} = \begin{bmatrix} \frac{\partial}{\partial x_1} \left(\frac{x_1}{C_b} \right) & -\frac{1}{C_{sp}} \\ \frac{\partial}{\partial x_1} (L_f y) & \frac{1}{C_{sp}^2 R_{sp}} \end{bmatrix}$$

$$\frac{\partial}{\partial x_1} \left(\frac{x_1}{C_b} \right) = \frac{1}{C_b} - \frac{x_1}{C_b^2 C_{Max}} (3C_0 SOC^2 + 2C_1 SOC + C_2)$$

$$\text{Let } \alpha = 3C_0 SOC^2 + 2C_1 SOC + C_2$$

$$\frac{\partial}{\partial x_1} \left(\frac{x_1 \alpha}{C_{Max} C_b^2} \right) = \frac{(x_1 \alpha)' C_b^2 - (x_1 \alpha) 2 C_b C_b'}{C_{Max} C_b^4} \quad \text{where } (\cdot)' \text{ is } \frac{\partial}{\partial x}$$

$$\frac{\partial}{\partial x_1} \left(\frac{1}{C_b} \right) = \frac{-\alpha}{C_{Max} C_b^2}$$

$$\frac{x_2}{C_{sp}^2} \frac{\partial}{\partial x_1} \left(\frac{1}{R_{sp}} \right) = \frac{R_1 R_2}{C_{Max} R_{sp}^2} exp\big(R_2(1 - SOC)\big)$$

$$\frac{\partial}{\partial x_1} (L_f y) = \left\{ \frac{\partial}{\partial x_1} \left(\frac{x_1 \alpha}{C_{Max} C_b^2} \right) - \frac{\partial}{\partial x_1} \left(\frac{1}{C_b} \right) \right\} i + \frac{x_2}{C_{sp}^2} \frac{\partial}{\partial x_1} \left(\frac{1}{R_{sp}} \right) \qquad (13)$$

The observability matrix *Obv* shown in equation (13) may be used to determine the conditions under which the state *x* is observable as well as in the computation of the observability condition number. The condition number is the ratio between the maximum and minimum singular values of *Obv* and may be used as a metric for observer performance.

3.3   Third-Order Model

Consider the third-order equivalent circuit model of [2] and shown in equation (14). Here the approximate discrete-time model is presented[i]. The added pair C_s and R_s capture the battery ohmic drop [2].

$$q_b(k) = q_b(k - 1) - i(k)T_s = f_1$$

$$q_{sp}(k) = q_{sp}(k-1) + \left(i(k) - q_{sp}(k-1)/\left(C_{sp}R_{sp}\right)\right)T_s = f_2$$

$$q_s(k) = q_s(k-1) + (i(k) - q_s(k-1)/(C_s R_s))T_s = f_3$$

$$SOC(k) = 1 - \frac{q_{max} - q_b(k)}{C_{max}}$$

$$R_{sp}(k) = R_{sp0} + R_{sp1}\exp\left(R_{sp2}(1 - SOC(k))\right)$$

$$C_b(k) = C_0 SOC(k)^3 + C_1 SOC(k)^2 + C_2 SOC(k) + C_3$$

$$V(k) = \frac{q_b(k)}{C_b} - \frac{q_{sp}(k)}{C_{sp}} - \frac{q_s(k)}{C_s} \tag{14}$$

As with the first and second-order systems, we compute *F* and *H* to form the EKF as shown in (15).

$$F = \frac{\partial f}{\partial x} = \begin{bmatrix} \dfrac{\partial f_1}{\partial x_1} & \dfrac{\partial f_1}{\partial x_2} & \dfrac{\partial f_1}{\partial x_3} \\ \dfrac{\partial f_2}{\partial x_1} & \dfrac{\partial f_2}{\partial x_2} & \dfrac{\partial f_2}{\partial x_3} \\ \dfrac{\partial f_3}{\partial x_1} & \dfrac{\partial f_3}{\partial x_2} & \dfrac{\partial f_3}{\partial x_3} \end{bmatrix} = \begin{bmatrix} 1 & 0 & 0 \\ \dfrac{\partial f_2}{\partial x_1} & 1 - \dfrac{T_s}{C_{sp}R_{sp}} & 0 \\ 0 & 0 & 1 - \dfrac{T_s}{C_s R_s} \end{bmatrix}$$

$$\frac{\partial f_2}{\partial x_1} = -\frac{x_2 T_s R_{sp1} R_{sp2}}{C_{sp} R_{sp}^2 C_{max}} exp\{R_{sp2}(1 - SOC)\}$$

$$H = \frac{\partial h}{\partial x} = \begin{bmatrix} \dfrac{\partial h}{\partial x_1} & \dfrac{\partial h}{\partial x_2} & \dfrac{\partial h}{\partial x_3} \end{bmatrix} = \begin{bmatrix} \dfrac{\partial}{\partial x_1}\left(\dfrac{x_1}{C_b}\right) & -\dfrac{1}{C_{sp}} & -\dfrac{1}{C_s} \end{bmatrix}$$

$$\frac{\partial}{\partial x_1}\left(\frac{x_1}{C_b}\right) = \frac{1}{C_b} - \frac{x_1}{C_b^2}\frac{\partial C_b}{\partial x_1}$$

$$\frac{\partial C_b}{\partial x_1} = \{3C_0 SOC^2 + 2C_1 SOC + C_2\}\frac{1}{C_{max}} \tag{15}$$

As with the first and second-order models, the observability matrix may be computed using the observable coordinates. This is rather lengthy and is not presented here. In practice the authors have observed that increasing the system order from second to third results in little gain in model accuracy. It is also noted that the computation of the observability indices is prone to error due to mathematical complexity.

3.4   Simplified Electrochemistry Model

The purpose of this section is to present a simplified electrochemistry model and to develop the EKF for state estimation and derive the observability matrix. The complete model is found in [5] and described in Appendix A.

The simple electrochemistry model considered here is the Nernst equation coupled with the Redlich-Kister expansion as shown in (16)[ii]. The physical meaning of each parameter is the same as given in the publication [5] [3] and reviewed in Appendix A.

$$q_{pS}(k) = q_{pS}(k-1) + i(k)T_s$$

$$q_{nS}(k) = q_{nS}(k-1) - i(k)T_s$$

$$x_{sp} = q_{pS}/q_{SMax} \qquad x_{sn} = q_{nS}/q_{SMax}$$

$$V_{INTp} = \frac{1}{nF}\sum_{j=0}^{N_p} A_{p,j}\left((2x_{sp}-1)^{j+1} - \frac{2x_{sp}j(1-x_{sp})}{(2x_{sp}-1)^{1-j}} \right)$$

$$V_{INTn} = \frac{1}{nF}\sum_{j=0}^{N_n} A_{n,j}\left((2x_{sn}-1)^{j+1} - \frac{2x_{sn}j(1-x_{sn})}{(2x_{sn}-1)^{1-j}} \right)$$

$$V_{Up} = U_{0p} + \frac{RT}{nF}\ln\left(\frac{1-x_{sp}}{x_{sp}}\right) + V_{INTp}$$

$$V_{Un} = U_{0n} + \frac{RT}{nF}\ln\left(\frac{1-x_{sn}}{x_{sn}}\right) + V_{INTn}$$

$$V = V_{Up} - V_{Un} \tag{16}$$

Like the Equivalent Circuit Models, we compute the matrixes *F* and *H* for the extended Kalman filter development as show in equation (17). Here the states are $z_1 = q_{pS}$ and $z_2 = q_{nS}$ and the EKF implementation is as shown in algorithm (6).

$$F = \frac{\partial f}{\partial x} = \begin{bmatrix} \dfrac{\partial f_1}{\partial z_1} & \dfrac{\partial f_1}{\partial z_2} \\ \dfrac{\partial f_2}{\partial z_1} & \dfrac{\partial f_2}{\partial z_2} \end{bmatrix} = \begin{bmatrix} 1 & 0 \\ 0 & 1 \end{bmatrix}$$

$$H = \frac{\partial V}{\partial z} = \begin{bmatrix} \dfrac{\partial V_{Up}}{\partial z_1} & -\dfrac{\partial V_{Un}}{\partial z_2} \end{bmatrix}$$

$$\frac{\partial V_{Up}}{\partial z_1} = \frac{RT}{nF}\left(\frac{1}{q_{SMax}x_{sp}(x_{sp}-1)}\right) + \frac{1}{nF}\sum_{j=0}^{N_p} A_{p,j}\left((j+1)(2x_{sp}-1)^j \frac{2}{q_{SMax}} \right)$$

$$- \frac{1}{nF}\sum_{j=0}^{N_p} A_{p,j}\left\{ \frac{2j(2x_{sp}-1)^{j-2}}{q_{SMax}}(-2x_{sp}^2 - 2jx_{sp}^2 + 2x_{sp} + 2jx_{sp} - 1) \right\}$$

$$\frac{\partial V_{Un}}{\partial z_2} = \frac{RT}{nF}\left(\frac{1}{q_{SMax}x_{sn}(x_{sn}-1)}\right) + \frac{1}{nF}\sum_{j=0}^{N_n} A_{n,j}\left((j+1)(2x_{sn}-1)^j \frac{2}{q_{SMax}} \right)$$

$$\tag{17}$$

8

$$-\frac{1}{nF}\sum_{j=0}^{N_n} A_{n,j}\left\{\frac{2j(2x_{sn}-1)^{j-2}}{q_{SMax}}\left(-2x_{sn}^2 - 2jx_{sn}^2 + 2x_{sn} + 2jx_{sn} - 1\right)\right\}$$

We next compute the observable coordinates h and $L_f h$ used to construct the observability matrix *Obv*. The observable coordinates are shown in equation set (18). Here we have taken advantage of the fact that the state equation is decoupled so we only show the development for the positive electrode in the computation of the derivatives; the negative electrode is the same.

$$f_1 = \dot{q}_{sp}(t) = i(t)$$
$$f_2 = \dot{q}_{sn}(t) = -i(t)$$
$$h = V = V_{Up} - V_{Un}$$
$$L_f h = \frac{\partial V_{Up}}{\partial z_1} f_1 - \frac{\partial V_{Un}}{\partial z_2} f_2 \tag{18}$$

The observability matrix is found by taking the Jacobian of the observable coordinates as shown in equation set (19). Here the continuous time model is used with states $\dot{q}_{sp}(t) = i(t)$, $\dot{q}_{sn}(t) = -i(t)$ and output equation $h(t) = V(t) = V_{Up}(t) - V_{Un}(t)$.

$$Obv = \nabla\begin{pmatrix} h \\ L_f h \end{pmatrix} = \begin{bmatrix} \dfrac{\partial h}{\partial z_1} & \dfrac{\partial h}{\partial z_2} \\ \dfrac{\partial L_f h}{\partial z_1} & \dfrac{\partial L_f h}{\partial z_2} \end{bmatrix} = \begin{bmatrix} \dfrac{\partial V_{Up}}{\partial z_1} & \dfrac{\partial V_{Un}}{\partial z_2} \\ \dfrac{\partial^2 V_{Up}}{\partial z_1^2} i & -\dfrac{\partial^2 V_{Un}}{\partial z_2^2} i \end{bmatrix}$$

$$\frac{\partial^2 V_{Up}}{\partial z_1^2} = \frac{-RT}{nFq_{SMax}^2}(x_{sp}^2 - x_{sp})^{-2}(2x_{sp} - 1) + \frac{4}{nFq_{SMax}^2}\sum_{j=0}^{N_p} A_{p,j}(j+1)j(2x_{sp}-1)^{j-1}$$

$$+ \frac{-4}{nFq_{SMax}^2}\sum_{j=0}^{N_p} A_{p,j}\,j(j-2)(2x_{sp}-1)^{j-3}\left(-2x_{sp}^2 - 2jx_{sp}^2 + 2x_{sp} + 2jx_{sp} - 1\right)$$

$$+ \frac{-4}{nFq_{SMax}^2}\sum_{j=0}^{N_p} A_{p,j}\,j(2x_{sp}-1)^{j-2}\left(-2x_{sp} - 2jx_{sp} + 1 + j\right)$$

$$\frac{\partial^2 V_{Un}}{\partial z_2^2} = \frac{-RT}{nFq_{SMax}^2}(x_{sn}^2 - x_{sn})^{-2}(2x_{sn} - 1) \tag{19}$$

In developing equation (19), it is assumed that $A_{n,j} = 0$ for all $j \neq 0$. The matrix *Obv* of equation (19) may be used to determine observability by considering the condition number.

4.   Battery Model Parameter Identification

The purpose of this section is to outline the methods used in identifying model parameters. Three sets of data will be used to identify the battery model variables. A description of the data is presented in Appendix B. The first set was obtained by slowly discharging a fully charged

battery and measuring the current and voltage. The second set was obtained based on a one C discharge (one C meaning that a fully charged battery rated at 1Ah should provide 1 ampere for one hour). The third set was obtained using a variable current discharge. The battery voltage and current profiles are presented in Appendix B. In all cases the battery voltage and current were recorded at a sampling rate of one hertz. Identification was performed in MATLAB using the Nelder-Mead nonlinear programming solver *fminsearch*. This section provides some information about the ordering of identification steps and plots demonstrating the quality of model fit for the training data.

4.1   Identification of Equivalent Circuit Model Parameters

The equivalent circuit battery model contains electrical components and empirical equations that are tuned to recreate the observed current-voltage dynamics of the battery. These battery parameters were identified by fitting a pulsed discharge laboratory experiment voltage profile with a Nelder-Mead downhill simplex method solution search that minimizes the error between the modeled and actual voltage profile. These identified parameters are associated with a selected battery from a batch of batteries of a given chemical formulation. These parameters are assumed to be unvaried across all similar battery packs of a given batch. Any differences in individual batteries due to manufacturing variation are accounted for by adaptation of the battery charge capacity term C_{max} of the C_b capacitor in the equivalent circuit model. A second fitting laboratory experiment to identify C_{max} is run by performing a 1/50 C slow discharge cycle for each battery. During this low current discharge cycle, the voltage across the C_b capacitor plays a dominant role. Thus, this experiment allows the C_{max} parameter in the equivalent circuit model to be fitted in isolation, also through use of the Nelder-Mead simplex method. According to the SOC definition C_{max} will always be less than q_{max}, due to electrochemical side-reactions that make some portion of a battery's charge carriers unavailable. The second low current experiment is necessary to satisfy issues raised by a Structural Identifiability analysis performed on a model with two RC network pairs that are locally, not globally, identifiable and may cause the estimation to oscillate between two distinct solutions [6].

Model parameters are found for the first-order model of equation set (1) using the slow discharge data set and a sample rate T_S of one hertz. To initialize these variables, information about the battery pack is obtained from the manufacturer and used to initialize the Nelder-Mead function *fminsearch*. Initialization is performed as shown below and the first set of model parameters is listed in Table 1. Here V_0 is found by averaging the first ten voltage readings at the beginning of the discharge, C_{Max} is the integral of the entire current history needed to discharge the battery, and q_{Max} is set slightly larger than C_{Max} in order to ensure *SOC* does not exceed one.

$$V_0 = mean(V(1:10)) \quad C_{Max} = \int i\,dt \quad q_{Max} = 1.02 C_{Max} \quad C_b = \frac{q_{Max}}{V_0} \quad C_3 = C_b - (C_0 + C_1 + C_2)$$

Parameter	Initial Guess	*fminsearch* Result
C_0	-2.2293e+02	-5.4926e+02
C_1	-3.2437e+02	2.7672e+02
C_2	3.71484e+03	3.1311e+03

Table 1. First-order battery parameters for Equivalent Circuit Model.

The data is run back through the resulting model to ensure a reasonable fit. The resulting output voltage and SOC estimations and are shown in Figure 2 and Figure 3. As can be seen in the figures, the resulting model closely approximates battery behavior for the slow discharge case. We see that the measured and estimated voltages are similar and that the SOC goes from fully charged (1) to fully discharged (0).
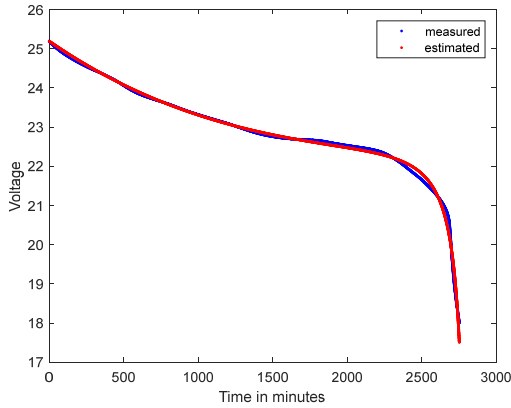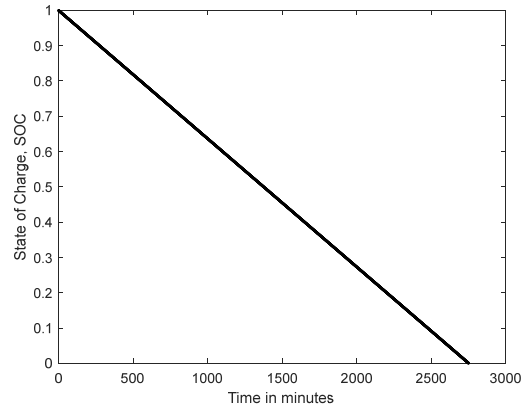

Figure 2. Battery Voltage.

Figure 3. State of Charge.

When the equivalent circuit model is extended to include an additional state, the original parameters from the first-order model are held constant and the additional parameters are identified using the one C discharge data. Here the second-order model is that of equation (9). The parameters to be identified are shown in Table 2 with the initial guess and results.

Parameter	Initial Guess	*fminsearch* Result
C_{sp}	316.69	1.0991e+02
R_{sp0}	0.0272	2.0130e-02
R_{sp1}	1.087e-3	3.1661e-20
R_{sp2}	34.64	4.3245e+01

Table 2. Second-Order Model.

As with the first-order model, the second-order model is checked with the data used for model identification to see if the fit is reasonable. The plots are shown in Figure 4 and Figure 5.
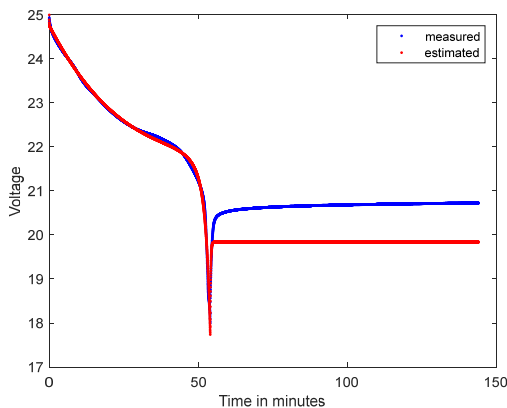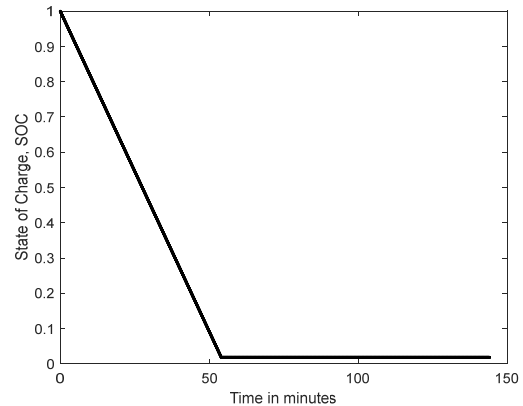

Figure 4. Battery Voltage.

Figure 5 State of Charge.

11

These figures demonstrate a reasonable fit. However, the recovery battery voltage does not reach that of the actual battery, and it is suspected that this is because the model is unable to capture battery dynamics when the battery current is zero.

The third-order battery model is investigated next. The additional parameters are shown in Table 3 and the model is equation (14). In determining the parameter values, a variable discharge was used.

Parameter	Initial Guess	*fminsearch* Result
R_s	0.32	2.4140e-15
C_s	39.06	2.0680e+14

Table 3. Battery Parameters for the Third-Order Model.

As with the first and second-order system, the fit is reasonable; see Figures 6 and 7.
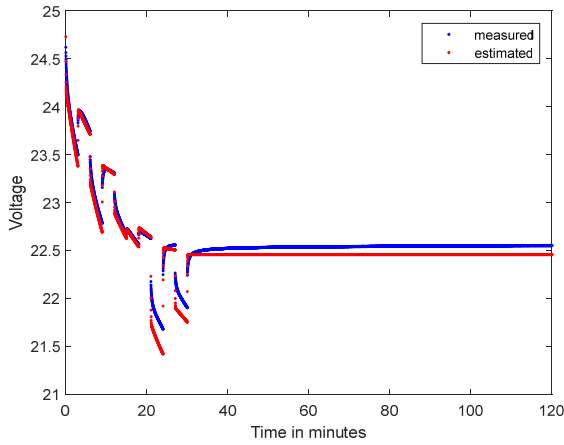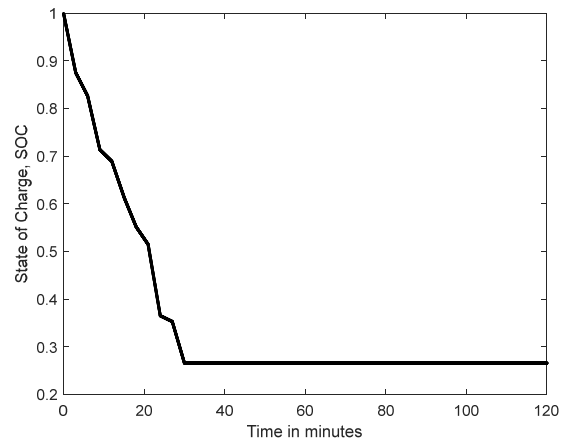

Figure 6. Battery Voltage.

Figure 7. State of Charge.

4.2 Identification of Electrochemistry Model Parameters

In this section we consider the identification of the electrochemistry model parameters as shown in equation (16). The electrochemistry model [5] is described in Appendix A. Parameter identification is a three-step process using a slow discharge data set, a one C data set, and a variable data set. The simplest electrochemistry model is the Nernst equation show in equation (20). This equation set is not used for battery modeling since it captures too few battery dynamics; but it is presented here for context and completeness.

$$q_{pS}(k) = q_{pS}(k-1) + iT_S \qquad q_{nS}(k) = q_{nS}(k-1) - iT_S$$

$$V_{Up} = U_{op} + \frac{RT}{nF}\ln\left(\frac{q_{SMax} - q_{pS}}{q_{pS}}\right) \qquad V_{Un} = U_{on} + \frac{RT}{nF}\ln\left(\frac{q_{SMax} - q_{nS}}{q_{nS}}\right)$$

$$V = V_{Up} - V_{Un}$$

$$SOC = \frac{q_{nS}}{0.6q_{Max}} \tag{20}$$

A more accurate battery model may be developed by adding the Redlich-Kister expansion to (20) as shown in equation (16). A summary of the constants and the variables to be identified by Nelder-Mead is presented in Table 4. More details about the electrochemistry model and

12

parameter meaning may be found in the literature [5]. In (16) R is the universal gas constant, n is one, T is the electrode temperature, and F is Faraday's constant. The model is initialized by setting $q_{SMax} = q_{Max}$, $q_{pS} = 0.4 q_{Max}$, and $q_{nS} = 0.6 q_{Max}$.

Parameter	Initial Guess	*fminsearch* Result
q_{Max}	1.3313e+05	1.5644e+05
U_{0p}	24.4559	2.3958e+01
U_{0n}	0.0522	5.3950e-02
A_{n0}	422.3000	8.3795e+02
A_{p0}	-269531	-3.5945e+05
A_p	0.4040, 168533, -563091, 63508, 2561180, 200182, -7825330, 1.2296e+04, 6861830, 2028170, -990957, -2602390;	6.0598e-01, 1.2516e+05, -5.1572e+05, -1.0277e+05, 2.5112e+06, 2.7440e+05, -9.6805e+06, 2.7031e+04, 1.0294e+07, 1.7921e+06, -1.2636e+05, -1.5294e+06

Table 4. Electrochemistry Battery Parameters.

Figure 8 and Figure 9 show the ability of the electrochemistry model to track the measured battery voltage and estimate the SOC. Performance is like the equivalent circuit model as shown in Figure 2. Although not shown in this paper, it is instructive to mention the variables
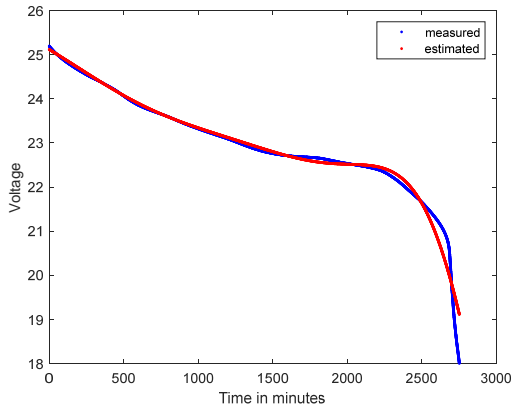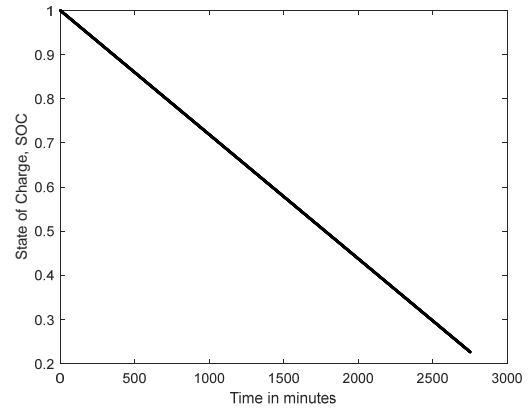

Figure 8. Battery Voltage.

Figure 9. State of Charge.

and parameter identification method used for the full electrochemistry model found in reference [5]. After the values of Table 4 are determined using the Nelder-Mead search based on (16) and the slow discharge data set, the remaining variables of the full electrochemical model of reference [5] may be used to find the remaining values by using the one C discharge data. These values are shown in Table 5.

Parameter	Initial Guess	*fminsearch* Result
$t_{Diffusion}$	9.2139e+04	1.2793e+06
R_0	0.0232	1.7270e-02
t_0	9.0276	1.4711e+01
t_{sp}	2.0911	2.7921e+01
k_p	260520	1.7408e+01
t_{sn}	3.1184e+04	6.0357e+05
k_n	1.7715e-29	5.5396e+06

Table 5. Electrochemistry Battery Parameters.

Although more complex, the electrochemistry model can be tuned to closely match battery dynamics. However, this complexity and exactness sacrifices robustness. The simpler models offer a less accurate model but are more forgiving of model tuning errors. The variable current data set is used to demonstrate the full electrochemistry model as shown in Figure 10 and Figure 11.
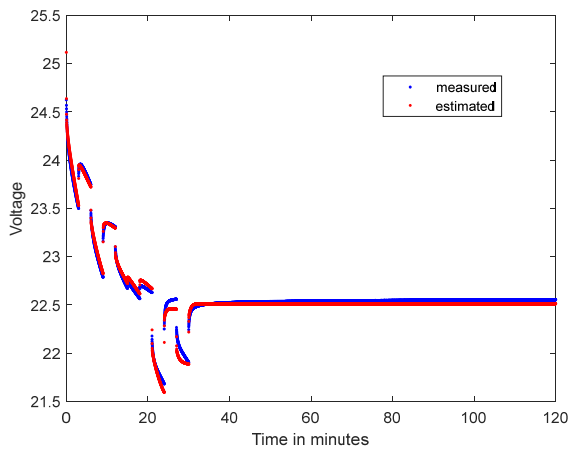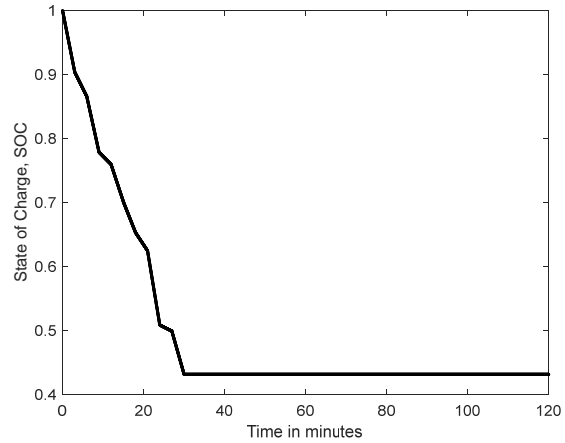

Figure 10. Battery Voltage.

Figure 11. State of Charge.

5.   State Observers and Observability

This section presents the application of the EKF observers and observability equations presented in Section 3. Three models are examined: the first and second-order equivalent circuit models, and the simplified electrochemistry model. For all three cases, plots showing estimator performance are presented followed by observability analysis.

5.1   Observer Performance for the Electrochemistry Model

As developed in Section 3, the EKF is used as the state observer. Figure 12 shows the plot of the estimated voltage using the EKF for the first-order equivalent circuit model. The data set used in this plot is the variable current set as described in Appendix B. Figure 13 is for the second-order equivalent circuit model. As can be seen in these figures, both observers track the measured voltage reasonably well, with the second-order model demonstrating superior estimation. The third order equivalent circuit model was also tried, but no noticeable gain in tracking ability was seen, so the plot is not presented here. The EKF model and measurement covariances were set to 0.1 and 0.001 for the first-order model respectively. The diagonal of the

Q matrix for the second-order model was set to [0.1, 0.01] and the measurement covariance *R* was set to 0.001. Estimated and measured voltages are shown in Figures 12 and 13. The measured voltage is the actual battery voltage, the model voltage is the voltage produced by the model with no EKF, and the estimated voltage is that produced by the EKF.
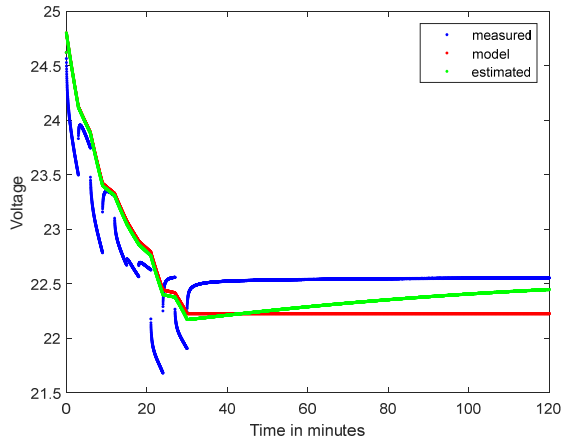

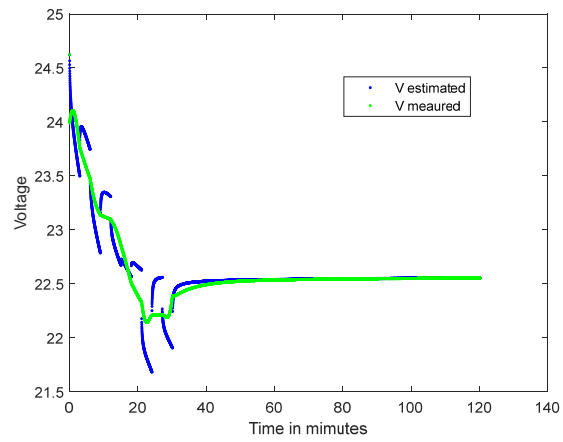Figure 12. Voltage, First-Order Equivalent Circuit Model.

Figure 13 Voltage, Second-Order Equivalent Circuit Model

The voltage plot for the electrochemistry model is show in Figure 14 for the variable discharge case. Also shown in Figure 15 are the two state estimations of the electrochemistry model. As we can see from these figures, the EKF does a reasonable job of tracking the internal battery states.
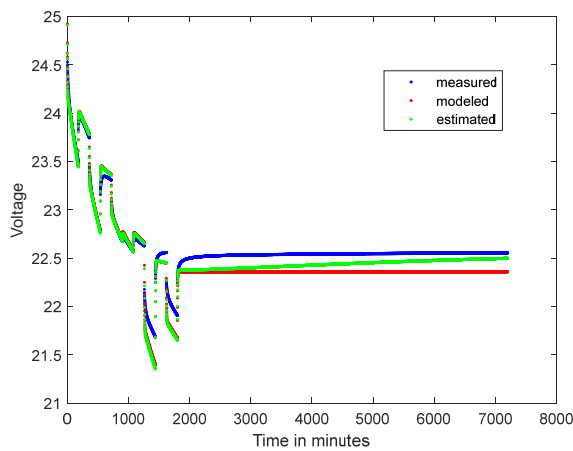

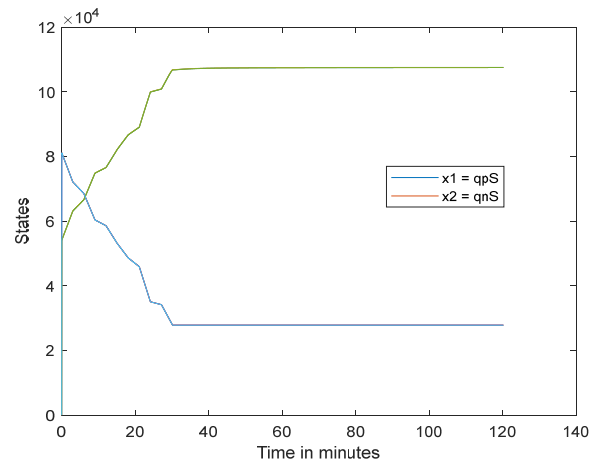Figure 14. Electrochemistry EKF Voltage.

Figure 15. State Estimates of Electrochemistry Model.

5.2   Observability

The observability of a nonlinear system may be determined by taking the Jacobian of the observable coordinates [4], as was done in Section 3. In this section we plot information about observability for both the first and second-order equivalent circuit models. For the first-order model, observability becomes weak when the scalar for the observability approaches zero. For our systems, this is a function of input as well as model characteristics. Three data sets are used to look at observability; slow discharge, one C discharge, and variable discharge. The

value for observability, *Obv*, is plotted with the discharge current for reference. These plots are shown in Figure 16, Figure 17, and Figure 18.
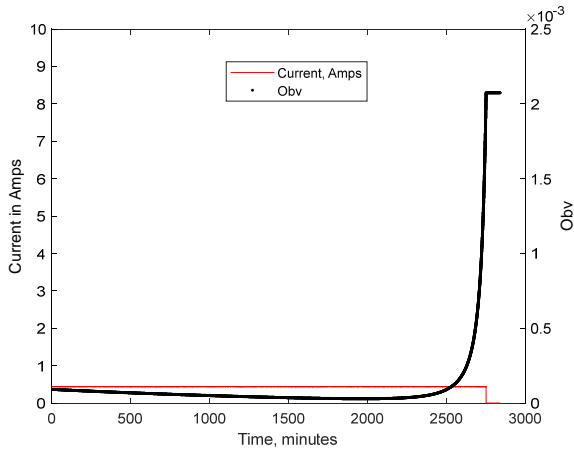

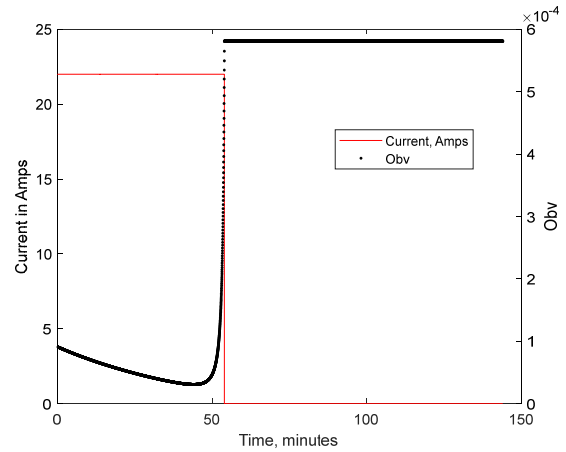Figure 16. Observability, First-Order, Slow Discharge.

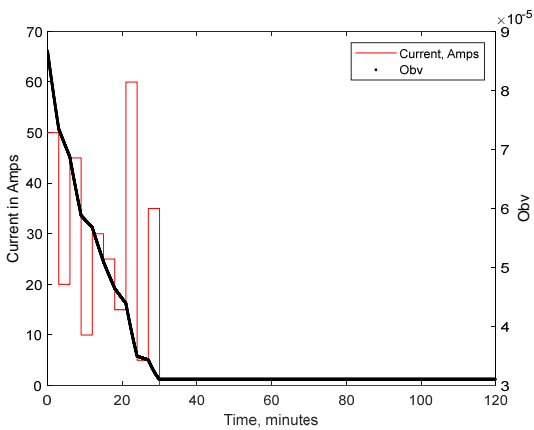Figure 17. Observability, First-Order, One-C Discharge.

Figure 18. Observability, First-Order, Variable Discharge.

From examining the plots, we see that *Obv* follows changes in the applied current. We are interested in the point where *Obv* goes to zero. The minimum values for *Obv* for each data set is 2.9132e-05, 3.0690e-05, and 3.1061e-05 respectively. Although somewhat weak, the first-order equivalent circuit model remains observable under the current values tested. A similar procedure may be applied to the second-order equivalent circuit model. Here we have a two by two observability matrix Obv. As a metric for observability, we take the condition number of Obv. The plots of the condition number and the current are shown in Figure 19, Figure 20, and Figure 21. The maximums of the condition number are at 723.8154, 723.2119, and 722.9001. There are no problems with observability for the currents tested; since the condition number is a ratio of the maximum singular value to the minimum, a large ratio would indicate weak observability.
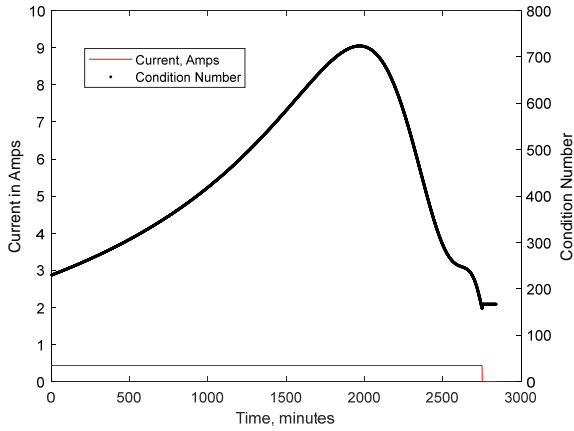
16

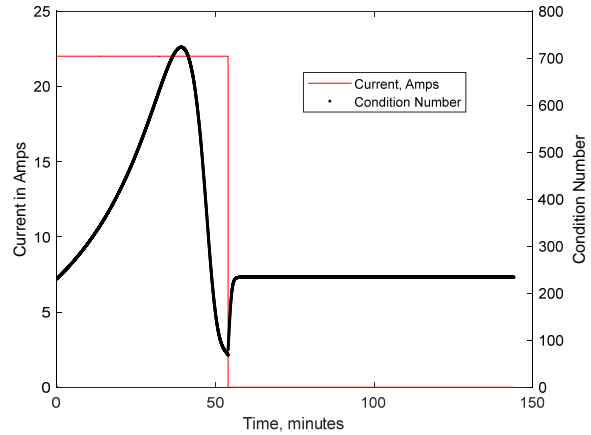Figure 19. Condition, Second-Order, Slow Discharge.

Figure 20 Condition, Second-Order, One-C Discharge.
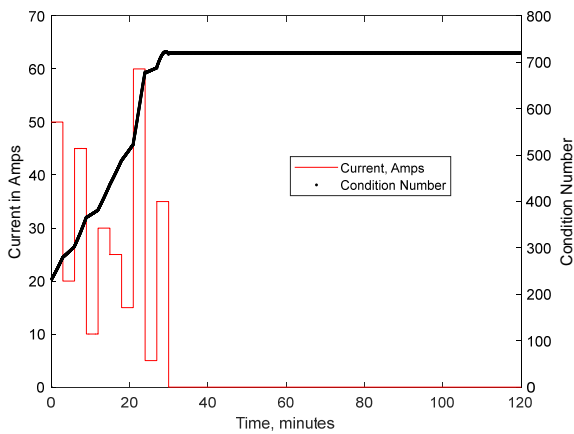

Figure 21 Condition, Second-Order, Variable Discharge

For observability of the electrochemistry model, consider the observability matrix in equation set (19). Here we see that both elements of the bottom row of *Obv* are zero when the current *i* draw is zero, making the matrix singular and the state unobservable when no current is drawn.

6 Experimental Flight Data

This section investigates the use of the EKF for state estimation using experimental data. The data was taken from a Polymer Li-ion battery during flight of an octocopter. The battery is rated at 22.2 V, 22000 mAh, 488.4 Wh and is manufactured by the Shenzhen Grepow Battery Co., LTD [7]. The battery parameters used here are those derived in Section 4.1 for the second-order equivalent circuit model. Figure 22 shows the octocopter and Figure 23 the battery.

Figure 22. Octocopter Used for Experimental Flight.   Figure 23. Battery Used for Flight.

From the figures below, we see that the battery model with EKF performed reasonably well and the condition number remained well bounded.
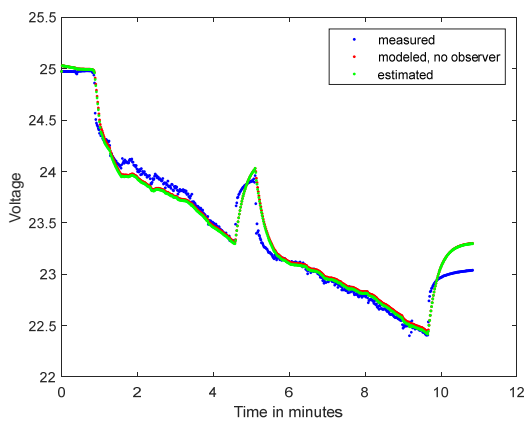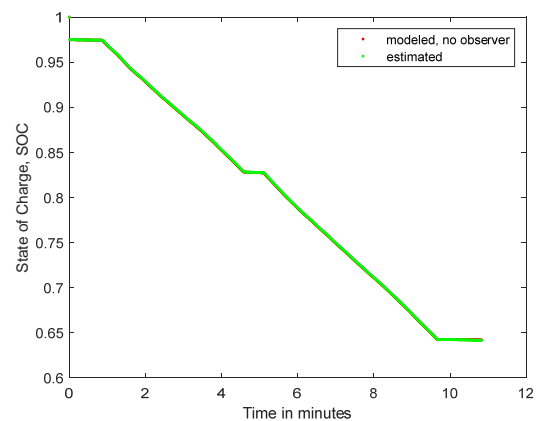

Figure 24. Battery Voltage.
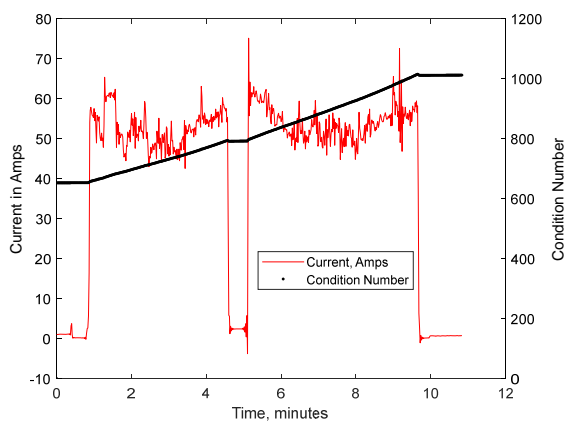

Figure 25 State of Charge.

Figure 26. Plot of Current and Condition Number.

18

Conclusions

The extended Kalman filter was developed for the equivalent circuit battery model. It was found that observability could be maintained at some level during battery usage. A simplified electrochemistry model was introduced, and observability explored. State observability was explored with both laboratory test data and data gathered during the flight of an octocopter. For the battery models examined, the extended Kalman filter offers a way to produce approximate state observations in real-time. However, the computation of the derivatives needed to implement the filter is tedious and prone to human error. Likewise, the computation of the derivatives needed to track observability is laborious.

References

[1] G. L. Plett, "Extended Kalman filtering for battery management systems of LiPB-based HEV battery packs, Part 1. Background, Part 2. Modeling and identification, Part 3. State and parameter estimation," *Journal of Power Sources,* vol. 134, pp. 252-261, 2004.

[2] M. Daigle and S. Sankararaman, "Predicting Remaining Driving Time and Distance of a Planetary Rover under Uncertainty," *ASCE-ASME J. Risk and Uncertainty in Engineering Systems, Part B: Mech. Engineering,* vol. 2, no. DO - 10.1115/1.4032848, 2016.

[3] M. Daigle, "Prognostics model library [computer software]," NASA, 2016. [Online]. Available: https://github.com/nasa/PrognosticsModelLibrary. [Accessed 2 September 2020].

[4] W. Yebin, H. Fang, L. Zhou and T. Wada, "Revisiting the State-of-Charge Estimation for Lithium-Ion Batteries, A Methodical Investigation of the Extended Kalman Filter Approach," *IEEE Control Systems Magazine,* Vols. 1066-033X, no. August, pp. 73-96, 2017.

[5] M. Daigle and C. S. Kulkarni, "Electrochemistry-based Battery Modeling for Prognostics," in *Annual Conference of the Prognostics and Health Management Society*, New Orleans, 2013.

[6] T. R. B. Grandjean, A. McGordon and P. A. Jennings, "Structural Identifiability of Equivalent Circuit Models for Li-Ion Batteries," *Energies,* vol. 10, no. 90, pp. 45-46, 2017.

[7] Shenzhen Grepow Battery Co., LTD, "https://community.openppg.com/ Material Safety Data Sheet Report No.: 17PNS01051 07001," 17 January 2017. [Online]. Available: https://community.openppg.com/uploads/short-url/yfEcb9SBzbTDBGCPTgdqwXu9rOU.pdf. [Accessed 2 September 2020].

[8] D. Karthikeyan, G. Sikha and R. White, "Thermodynamic Model Development for Lithium Intercalation Electrodes," *Journal of Power Sources,* vol. 185, no. 2, pp. 1398-1407, 2008.

[9] M. Daigle, "End-of-discharge and End-of-life Prediction in Lithium-ion Batteries with Electrochemistry-based Aging Models," in *American Institute of Aeronautics and Astronautics*, San Diego, 2016.

[10] S. Särkkä, Bayesian Filtering and Smoothing, New York: Cambridge University Press, 2013.

[11] S. J. Julier and J. K. Uhlmann, "A new extension of the kalman filter to nonlinear systems," in *AeroSense: The 11th International Symposium on Aerospace/Defence Sensing, Simulation and Controls*, 1997.

Appendix A

The basic kinetics for the electrochemistry model is derived from the chemical reactions that take place at the electrodes and are shown in equations A.1 through A.4 [5]. Equations A.1 and A.2 are the reactions at the electrodes during a discharge. During discharge, an oxidation reaction takes place at the negative electrode resulting in lithium-ions and electrons. The electrons travel from the surface of the negative electrode to the surface of the positive electrode leaving the surface potential of the negative electrode increased and the surface potential of the positive electrode decreased causing them to converge towards the same potential. This means that the voltage will decrease as the voltage across the battery is the difference between the negative electrode surface potential and the positive electrode surface potential. The lithium-ions travel from the bulk of the negative electrode to the bulk of the positive electrode through the electrolyte. A reduction reaction occurs at the positive electrode when lithium-ions diffuse into the surface and the electrons diffuse into the bulk. The result is the increase in the surface potential at the positive electrode which counters the decrease from the initial introduction of the electrons.

$$Li_xC \rightarrow C + xLi^+ + xe^- \tag{A.1}$$

$$Li_{1-x}CoO_2 + xLi^+ + xe^- \rightarrow LiCoO_2 \tag{A.3}$$
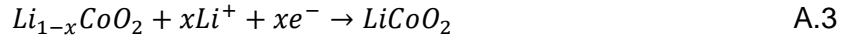
Equations A.3 and A.4 are the reactions that take place at the electrodes during charge. During charge, oxidation occurs at the positive electrode and results in lithium-ions and electrons as products. The electrons travel from the surface of the positive electrode to the surface of the negative electrode resulting in an increase in the surface potential at the positive electrode and a decrease in the surface potential at the negative electrode. The surface potentials diverge during charge which increases the voltage. The lithium-ions travel from the bulk of the positive electrode to the bulk of the negative electrode through the electrolyte. A reduction reaction takes place at the negative electrode when lithium-ions diffuse into the surface and electrons diffuse into the bulk. This results in an increase in the surface potential at the negative electrode which counters the decrease in potential from the introduction of the electrons that traversed from the positive electrode surface.

$$C + xLi^+ + xe^- \rightarrow Li_xC \tag{A.3}$$

$$LiCoO_2 \rightarrow Li_{1-x}CoO_2 + xLi^+ + xe^- \tag{A.4}$$
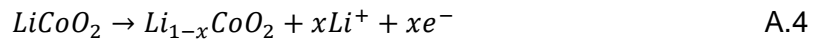
To define the electrochemistry-based model, the relevant voltages and how they impact the voltage of the battery must be detailed. First, the battery voltage that the model is capturing and our system is measuring is seen in Figure A.1 [5] to be the difference in potential between the surfaces of the negative and positive electrodes.

The voltages that factor into the determination of the battery voltage can be stated in relation to how they detract from the ideal voltage. This voltage is defined as the difference between $V_{U,p}$ and $V_{U,n}$. The first set of voltages that detract from the equilibrium voltage are known as ohmic voltage drops. The ohmic voltages are comprised of the electrolyte ohmic voltage denoted V_e,
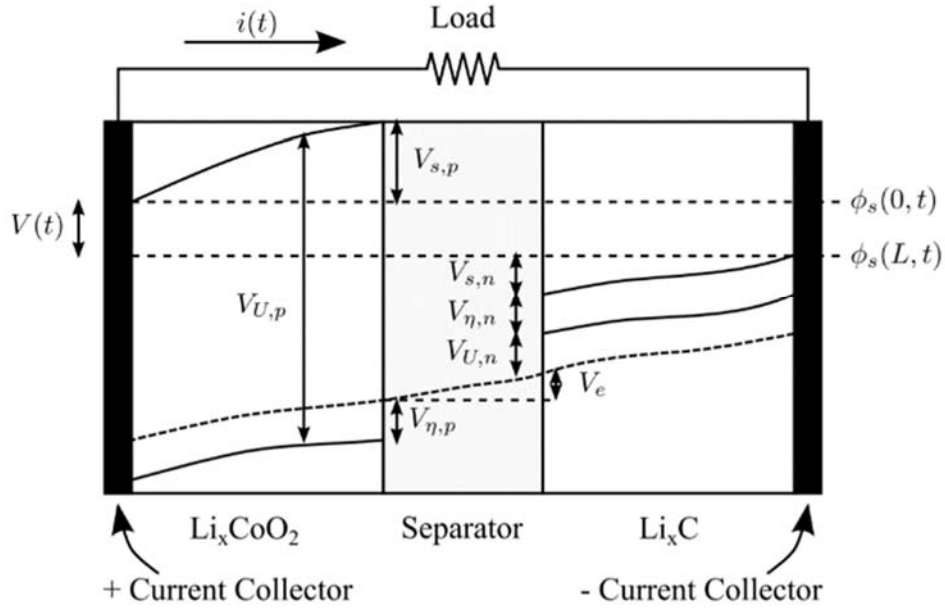
Figure A.1. Battery Diagram.

the solid phase ohmic voltage of the positive electrode denoted $V_{s,p}$, and the solid phase ohmic voltage of the negative electrode denoted $V_{s,n}$. The second set of voltages that detract from the equilibrium voltage are known as surface overpotentials and are a result of charge transfer resistance and solid electrolyte interface kinetics [5]. The surface overpotentials are comprised of a negative electrode surface overpotential denoted $V_{\eta,p}$ and a positive electrode surface overpotential denoted $V_{\eta,n}$.

The state definition, the input, the output, and the relevant model variables are defined in equations A.5 through A.7. The state vector is defined in equation A.5 and consists of the positive electrode surface charge $q_{s,p}$, the positive electrode bulk charge $q_{b,p}$, the negative electrode bulk charge $q_{b,n}$, the negative electrode surface charge $q_{s,n}$, the sum of the ohmic voltage contributions V_o', the positive electrode overpotential $V_{\eta,p}'$, and the negative electrode overpotential $V_{\eta,n}'$. The input vector is defined in equation C.6 and consists of the discharge current i_{app}. The output vector is defined in equation A.7 and consists of the battery voltage V.

$$x(t) = [\, q_{s,p} \; q_{b,p} \; q_{b,n} \; q_{s,n} \; V_o' \; V_{\eta,p}' \; V_{\eta,n}' \,] \tag{A.5}$$

$$u(t) = [\, i_{app} \,] \tag{A.6}$$

$$y(t) = [\, V \,] \tag{A.7}$$

The state transition equations for the electrode charges incorporate the discharge current and diffusion, as shown in equations A.8 through A.12 [5]. Inter-electrode electron flow occurs primarily at the surface of the electrodes. Hence, the current does not have a direct impact on charge at the bulk of the electrodes. Indirectly, the current changes the concentration gradient of lithium-ions between the surface and the bulk of the electrodes which impacts diffusion and in turn the charge at the bulk of the electrodes. The cumulative charge equations are shown in equations A.13 through A.15 [5].

$$\dot{q}_{s,p} = i_{app} + \dot{q}_{bs,p} \tag{A.8}$$

$$\dot{q}_{b,p} = -\dot{q}_{bs,p} \tag{A.9}$$

$$\dot{q}_{b,n} = -\dot{q}_{bs,n} \tag{A.10}$$

$$\dot{q}_{s,n} = -i_{app} + \dot{q}_{bs,n} \tag{A.11}$$

$$\dot{q}_{bs,i} = \frac{1}{D}(c_{b,i} - c_{s,i}) \quad i = p, n \tag{A.12}$$

$$q_p = q_{s,p} + q_{b,p} \tag{A.13}$$

$$q_n = q_{s,n} + q_{b,n} \tag{A.14}$$

$$q_{max} = q_p + q_n \tag{A.15}$$

These charge equations are coupled directly with the concentration and lithium mole fraction equations shown in equations A.16 through A.20 [5]. Here v refers to volume and the subscript i refers to either electrode. The lithium-ion mole fraction for the positive electrode must be at least 0.4 and the lithium-ion mole fraction at the negative electrode must be no more than 0.6. If the positive electrode has a mole fraction of lithium less than 0.4, lithium cannot be reversibly removed [8]. The mole fractions at the positive electrode and negative electrode are complimentary so together they must add to 1. Hence, the mole fraction at the negative electrode must be no greater than 0.6.

$$c_{b.i} = \frac{q_{b.i}}{v_{b.i}} \tag{A.16}$$

$$c_{s,i} = \frac{q_{s,i}}{v_{s,i}} \tag{A.17}$$

$$x_i = \frac{q_i}{q_{max}} \tag{A.18}$$

$$x_{s,i} = \frac{q_{s,i}}{q_{s,i,max}} \tag{A.19}$$

$$x_{b,i} = \frac{q_{b,i}}{q_{b,i,max}} \tag{A.20}$$

The equations to solve for the cumulative ohmic voltage, the surface overpotentials, and the intermediate variables are shown in equations A.21 through A.29 [5] [9]. In equation A.21, U_0 is the reference potential. In equations A.21 through A.29, R is the universal gas constant, T is the electrode temperature, n is the number of electrons transferred in from the chemical reaction in equation A.1, and F is Faraday's constant. R_o is the cumulative resistance from the ohmic voltages drop, α is the symmetry factor, and S_i is the area of the electrode. The terms $\tau_{\eta,p}$, and $\tau_{\eta,n}$ denote time constants. Lastly, $A_{i,k}$ are parameters for the Redlich-Kister expansion. The Redlich-Kister expansion is used to capture the activity coefficient terms related to excess Gibbs free energy [8]. For a more detailed outline of the intermediate variables see [5].

$$V_{u,i} = U_{0,i} + \frac{RT}{nF}\ln\left(\frac{1 - x_{s,i}}{x_{s,i}}\right) + V_{INT,i} \tag{A.21}$$

$$V_{INT,i} = \frac{1}{nF}\sum_{k=0}^{N_i} A_{i,k}\left((2x_{s,i} - 1)^{k+1} - \frac{2x_{s,i}k(1 - x_{s,i})}{(2x_{s,i} - 1)^{1-k}}\right) \tag{A.22}$$

$$V_o = i_{app}R_o \qquad\qquad\text{A.23}$$

$$V_{\eta,i} = \frac{RT}{F\alpha}\operatorname{arcsinh}\left(\frac{J_i}{2J_{i0}}\right) \qquad\qquad\text{A.24}$$

$$J_i = \frac{i_{app}}{S_i} \qquad\qquad\text{A.25}$$

$$J_{i0} = k_i(1 - x_{s,i})^\alpha (x_{s,i})^{1-\alpha} \qquad\qquad\text{A.26}$$

$$\dot{V}_o' = \frac{V_o - V_o'}{\tau_o} \qquad\qquad\text{A.27}$$

$$\dot{V}_{\eta,p}' = \frac{V_{\eta,p} - V_{\eta,p}'}{\tau_{\eta,p}} \qquad\qquad\text{A.28}$$

$$\dot{V}_{\eta,n}' = \frac{V_{\eta,n} - V_{\eta,n}'}{\tau_{\eta,n}} \qquad\qquad\text{A.29}$$

The equation for the battery voltage is shown in equation A.30 and the state of charge equations are shown in equations A.31 and A.32 [5]. The nominal state of charge refers to the percent of charge left at the negative electrode while the apparent state of charge refers to the percent of charge left at the surface of the negative electrode. If the charge at the surface of the negative electrode becomes entirely depleted, discharge cannot continue until charge diffuses from the bulk of the negative electrode so long as the nominal state of charge has not been entirely depleted in that instance.

$$V = V_{u,p} - V_{u,n} - V_o' - V_{\eta,p}' - V_{\eta,n}' \qquad\qquad\text{A.30}$$

$$SOC_{nominal} = \frac{q_n}{0.6q_{max}} \qquad\qquad\text{A.31}$$

$$SOC_{apparent} = \frac{q_{s,n}}{0.6q_{s,n,max}} \qquad\qquad\text{A.32}$$

Appendix B

This appendix describes the battery data used for parameter identification and modeling analysis. Four data sets were created using a Maccor 4000 battery cycler. The first data set was found to have corrupted data and data set two is presented in Figure B.1, Figure B.2, and Figure B.3. In these figures blue is the battery voltage and red the current. Data set two is presented here because it is the one used in the battery model simulations. For the flight data, battery four was used.

The red lines in the figures are the current values labeled on the right axis. For the slow discharge, the current was held at around 0.44 amperes; for the 1 C discharge the current was held around 22 amperes, and for the variable discharge case the current went through quantized steps as can be seen in the red line shown in Figure B.3.
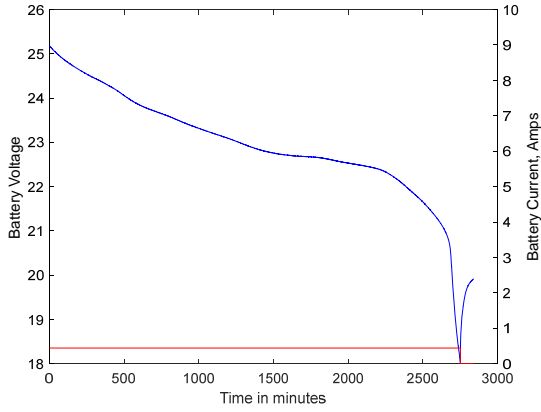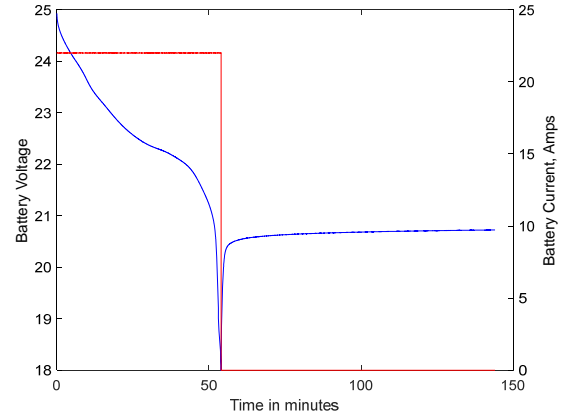
Figure B.1. Slow Discharge.
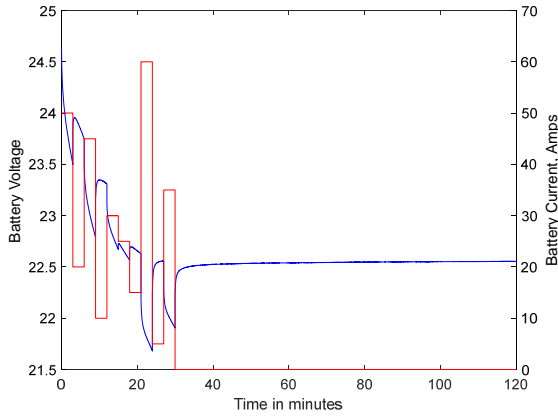

Figure B.1. One-C Discharge.

Figure B.3. Variable Discharge.

---

[i] The exact form is $A = \begin{bmatrix} 1 & 0 & 0 \\ 0 & \exp\left(\frac{-T_s}{C_{sp}R_{sp}(k)}\right) & 0 \\ 0 & 0 & \exp\left(\frac{-T_s}{C_s R_s}\right) \end{bmatrix}$ and $B = \begin{bmatrix} -T_s \\ C_{sp}R_{sp}(t)\left(1 - \exp\left(\frac{-T_s}{C_{sp}R_{sp}(k)}\right)\right) \\ C_s R_s(t)\left(1 - \exp\left(\frac{-T_s}{C_s R_s(k)}\right)\right) \end{bmatrix}$

[ii] Here the discrete-time approximation is exact, with $A = \begin{bmatrix} 1 & 0 \\ 0 & 1 \end{bmatrix}$ and $B = \begin{bmatrix} 1 \\ -1 \end{bmatrix}$ and state defined as $\begin{bmatrix} q_{pS}(k) \\ q_{nS}(k) \end{bmatrix}$

REPORT DOCUMENTATION PAGE

The public reporting burden for this collection of information is estimated to average 1 hour per response, including the time for reviewing instructions, searching existing data sources, gathering and maintaining the data needed, and completing and reviewing the collection of information. Send comments regarding this burden estimate or any other aspect of this collection of information, including suggestions for reducing the burden, to Department of Defense, Washington Headquarters Services, Directorate for Information Operations and Reports (0704-0188), 1215 Jefferson Davis Highway, Suite 1204, Arlington, VA 22202-4302. Respondents should be aware that notwithstanding any other provision of law, no person shall be subject to any penalty for failing to comply with a collection of information if it does not display a currently valid OMB control number.
PLEASE DO NOT RETURN YOUR FORM TO THE ABOVE ADDRESS.

1. REPORT DATE *(DD-MM-YYYY)*	2. REPORT TYPE	3. DATES COVERED *(From - To)*
1-01-2021	Technical Memorandum	

4. TITLE AND SUBTITLE

Mathematical Characterization of Battery Models

5a. CONTRACT NUMBER

5b. GRANT NUMBER

5c. PROGRAM ELEMENT NUMBER

6. AUTHOR(S)

Eure, Kenneth W.; Hogge, Edward F.

5d. PROJECT NUMBER

5e. TASK NUMBER

5f. WORK UNIT NUMBER

340428.02.20.07.01

7. PERFORMING ORGANIZATION NAME(S) AND ADDRESS(ES)

NASA Langley Research Center
Hampton, VA 23681-2199

8. PERFORMING ORGANIZATION REPORT NUMBER

9. SPONSORING/MONITORING AGENCY NAME(S) AND ADDRESS(ES)

National Aeronautics and Space Administration
Washington, DC 20546-0001

10. SPONSOR/MONITOR'S ACRONYM(S)

NASA

11. SPONSOR/MONITOR'S REPORT NUMBER(S)

NASA-TM-20205008059

12. DISTRIBUTION/AVAILABILITY STATEMENT

Unclassified
Subject Category
Availability: NASA STI Program (757) 864-9658

13. SUPPLEMENTARY NOTES

14. ABSTRACT

.Kalman Filter as a tool for battery state estimation and the estimation of battery state of charge. The mathematical details based on the equivalent circuit model are presented followed by an electrochemical engineering model. A simplified first-order model is used to demonstrate the procedure followed by second and third-order models. Next a simplified electrochemistry model is presented along with observer development. State observability is calculated for the simpler equivalent circuit models and the simplified electrochemistry model. An outline of the battery model parameter identification method is presented, and model performance based on experimental and flight data is demonstrated.

15. SUBJECT TERMS

Air Transportation and Safety

16. SECURITY CLASSIFICATION OF:			17. LIMITATION OF ABSTRACT	18. NUMBER OF PAGES	19a. NAME OF RESPONSIBLE PERSON
a. REPORT	b. ABSTRACT	c. THIS PAGE			STI Help Desk (email: help@sti.nasa.gov)
U	U	U	UU	30	19b. TELEPHONE NUMBER *(Include area code)* (757) 864-9658